9
CFD Simulation of Large Hydrocarbon and Peroxide Pool Fires

Axel Schönbucher, Stefan Schälike, Iris Vela, and Klaus-Dieter Wehrstedt

9.1
Introduction

Accidental fires in process industries often occur as pool fires, which are hazardous to people and adjacent objects because of thermal radiation, largely sooting plumes and formation of other combustion products [1–3]. In addition to experimental pool fire tests, numerical investigation of these fires using Computational Fluid Dynamics (CFD) codes is becoming more important. In regard to safety, thermal radiation is one of the main interests in pool fire research. The Surface Emissive Power (SEP) is a key parameter to characterize thermal radiation emitted by a fire. The derived quantity SEP is usually defined as the heat flux due to thermal radiation in relation to flame surface A_F. As well as the SEP, the temperatures T and irradiances E of pool fires are of particular interest. CFD simulation of large pool fires is helpful for a better understanding of fire dynamics and to reduce the number of large-scale experiments. To predict the thermal radiation from the jet engine fuel JP-4 ($d = 2$, 8, 16 and 25 m) and DTBP (di-*tert*-butyl peroxide, $d = 1.12$ and 3.4 m) pool fires CFD methods are used, and the CFD results are compared with experiments.

9.2
Governing Equations

The rate of change of extensive properties, such as mass, momentum, energy or species mass, of a given quantity of matter can be described by conservation laws [4–6]. Assuming the control volume to become infinitesimally small leads to a differential form of the species mass equation:

$$\frac{\partial \varrho_i}{\partial t} = -\mathrm{div}(\varrho_i \vec{u}) - \mathrm{div}\,\vec{j}_i + M_i r_i. \tag{9.1}$$

In a combustion process with diluted gases, a consistent diffusion coefficient for all species is suitable, while thermo-diffusion (Soret effect) and pressure diffusion can be neglected, and mass flux density is given by Fick's 1st law [7]. Setting the

Process and Plant Safety: Applying Computational Fluid Dynamics, First Edition. Edited by J. Schmidt.

models, for example, the Magnussen model [28], the Tesner model [29], the Lindstedt model [30], or the Moss-Brookes model [31].

Of special engineering interest are the incident radiation G, radiative heat flux q_{rad}, and radiative source term div q_{rad}, which are derived from the following integrals and are discretized, for example, with Discrete Ordinates model (DO) [32, 33]:

$$G = \int_{4\pi\Omega_0} L(\vec{s})\mathrm{d}\Omega \approx \sum_m w_m L_m, \; q_{rad} = \int_{4\pi\Omega_o} L(\vec{s})\vec{s}\mathrm{d}\Omega \approx w_m L_m \vec{s},$$

$$\text{and} \quad \mathrm{div}\, q_{\mathrm{rad}} = a_{\mathrm{eff}}(4\pi L_b - G). \tag{9.23}$$

The Discrete Transfer model (DT, [34]) and the Monte Carlo model (MC, [35]) are also used in the present chapter.

9.6 CFD Simulation

In CFD simulation, a domain is represented by a 3-D hexahedral block structured mesh [36–39] (Figure 9.2). The fuel is assumed to be already evaporated, and the fuel vapor entering the domain from the inlet has a constant temperature of $T = T_b$ and an experimentally determined constant mass flux. The inlet is surrounded by a low rim and an adiabatic ground area. The remaining boundary conditions are set as 'opening pressure' (CFX) and 'pressure outlet' (FLUENT) at a relatively large distance from the pool to achieve open boundary conditions. With increasing axial und vertical distance from the pool, cell size increases.

The time steps vary, depending on sufficient convergence from $t = 10^{-6}$s to $t = 10^{-4}$s, depending on the Courant-Friederich-Levy (CFL) criterion. In the pool fire simulations presented here, the following sub-models are used:

- Assumed pdf approach with laminar flamelets containing up to 112 species and 800 elementary reactions and eddy dissipation model.
- Lindstedt, Tesner, or Moos-Brookes soot model.
- Monte Carlo, Discrete Transfer, and Discrete Ordinates models for radiation.

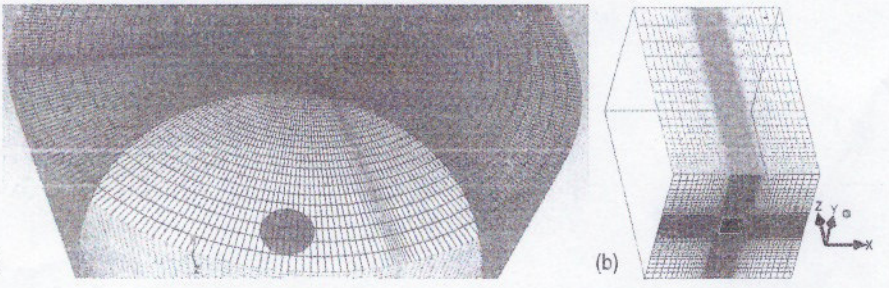

Figure 9.2 Block structured grid for simulation of (a) JP-4 (b) DTBP pool fires.

Table 9.1 Starting and boundary conditions of CFD pool fire simulation.

Starting Conditions		Boundary Conditions	
Quantity	Value		
Mass fraction N_2	0.743	Upper end face	$p = p_a$
Mass fraction O_2	0.231	+ Lateral area	298 K
Mass fraction Ar	0.012	'Pressure outlet'	Open boundary conditions
Mass fraction CO_2	0.001		
Mass fraction H_2O	0.013	Lower end face	Adiabatic
p_a	1013.25 hPa	+ Pool rim	Heat flux to pool rim
$p-p_a$	0	'Wall'	$\dot{q} = 0$
Flow velocity	$u_x = u_y = u_z = 0$		
Temperature	298 K	Pool	Experimentally determined
Gravitational acceleration	$9.81\ m\ s^{-2}$	'Mass flow inlet'	Mass burning rate
Mixing fraction f	$f = 0$		$p = p_a$, $T = T_b$

The coupling between thermal radiation and soot reactions is described either by a modified effective absorption coefficient or a weigted sum of gray gases approach. For JP-4 pool fires, a four-step discontinuity function is used which includes the experimentally determined organized structures of the fire: effective reaction zone, hot spots, and soot particles. Again in DTBP pool fires, a weighted sum of gray gases model is applied for coupling thermal radiation and soot reactions.

The governing equations were solved by an iterative solution method with either coupled or segregated solvers, for example, the pressure correction methods SIMPLE (Semi-Implicit Methods for Pressure-Linked Equations). The starting and boundary conditions are listed in Table 9.1.

The main purpose is to determine the temperature T, Surface Emissive Power SEP and irradiance E. The simulations are started with a two-equation model based on the eddy viscosity hypothesis, such as $k-\varepsilon$ with a buoyancy correction term to reach a certain flame height which refers to the developing stage of the fire. Assuming the flame to be developed, further simulation is continued by using Scale-Adaptive Simulation (SAS) and Large Eddy Simulation (LES). CFD simulation is carried out with commercial software ANSYS CFX 11 [40] and ANSYS FLUENT 12 [41].

9.7 Results and Discussion

9.7.1 Flame Temperature

A quantitative description of JP-4 pool fire dynamics ($d = 16$ m and 25 m) is shown in Figure 9.3 by the simulated temperature fields. In these fields the flame pulsation is noticeable. The flame pulsation is connected with a formation and rising of vortices

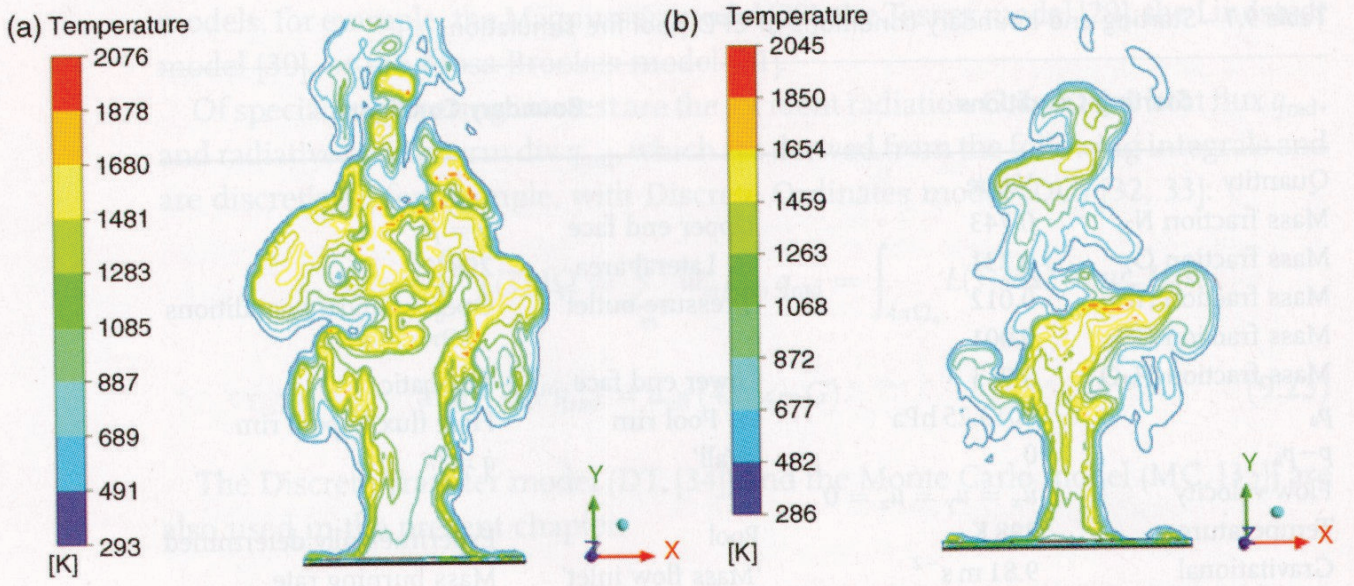

Figure 9.3 CFD-predicted instantaneous temperature fields of JP-4 pool fire (a) $d = 16$ m; (b) $d = 25$ m.

which greatly affects the location of the maximum flame temperature. Inside the vortices the temperatures are significantly higher (2100 K $\leq T \leq$ 1800 K) than in the outside area (1200 K $\leq T \leq$ 1800 K). Hot flame gases have a significantly lower density and therefore a rise in hot volumes is observable with increasing time. As a consequence, the flame surface is cooled down by air entrainment, so that the temperature in the upper part of the flame is lower. The comparison of small ($d = 2$ m) and large scale ($d \geq 16$ m) JP-4 pool fires shows that the maximum temperatures in the flames are more and more shifted in the direction of the pool surface because of the frequent occurrence of hot spots near the pool surface. Analyzing the instantaneous results, it can be seen that in case of a JP-4 pool fire with $d = 2$ m the maximum temperatures are visible in the upper part of the flame (due to the more frequent occurrence of hot spots). In the case of a JP-4 fire with larger pool diameter ($d = 16$ m and 25 m), maximum temperatures are located near the pool and the inside of the lower vortices.

Pulsation of flames occurs in all simulations, although with different frequencies. This has an influence on the SEP of the flame and also on the irradiance to surrounding areas and people. In Figure 9.3, the constriction of the flame between the clear combustion zone and the plume zone is visible. Up to the borderline which separates the combustion zone from the upper plume zone higher temperatures are found. Above this the flame temperature significantly decreases.

JP-4 pool fires show a decreasing maximum time-averaged flame temperature $\bar{T}$ with increasing pool diameter. Temperatures $\bar{T}$ of 1280 K ($d = 2$ m), 1250 K ($d = 8$ m), 1230 K ($d = 16$ m) and 1200 K ($d = 25$ m) are obtained by CFD.

The CFD-predicted instantaneous temperature fields of DTBP pool fires are shown in Figure 9.4.

For DTBP pool fires, CFD maximum axial time-averaged flame temperatures [$\bar{T}$ of 1410 K ($d = 1.12$ m) and 1520 K ($d = 3.4$ m)] (Figure 9.5) agree well with the experimental results [1500 K ($d = 1.12$ m) and 1580 K ($d = 3.4$ m)].

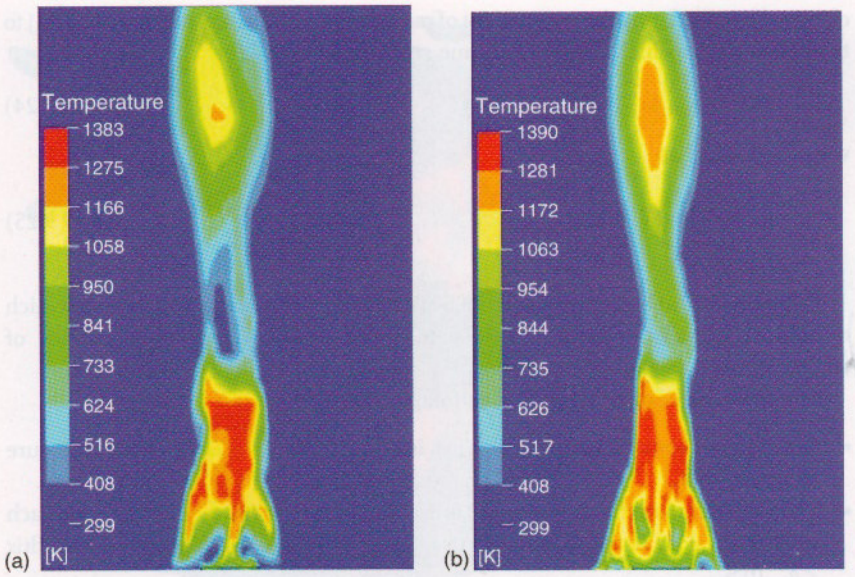

Figure 9.4 CFD predicted instantaneous temperature fields of DTBP pool fires (a) $d = 1.12$ m; (b) $d = 3.4$ m.

9.7.2
Surface Emissive Power (SEP)

The SEP is a derived quantity, and its value depends on flame surface and flame shape. Especially the value of the flame height, but also atmospheric transmission and general experimental errors are import. The SEP of a fire can be obtained by CFD simulation in three ways. In the first way the SEP is predicted by the radiative heat flux q_{out} leaving each grid cell placed on the flame surface A_F. The value of q_{out} can by

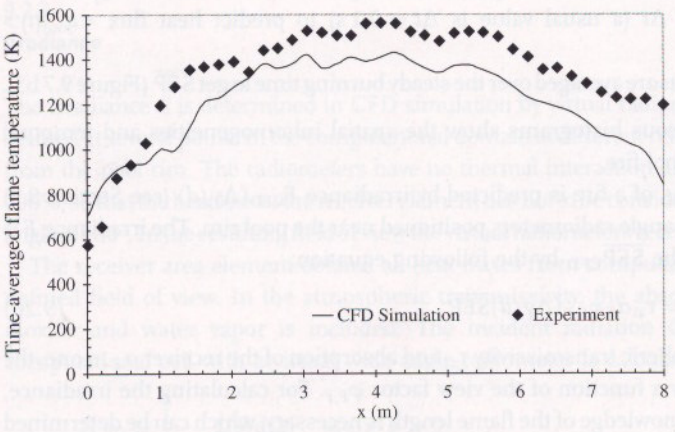

Figure 9.5 Time-averaged axial temperature profiles of DTBP ($d = 3.4$ m).

CFD zur Simulation großer Kohlenwasserstoff/Peroxid-Poolfeuer

A. Schönbucher, S. Schälike, I. Vela, K.-D. Wehrstedt

Lehrstuhl für Technische Chemie I, Universität Duisburg-Essen und
Fachgruppe 2.2 Reaktionsfähige Stoffe und Stoffsysteme, BAM Berlin

50. Tutzing-Symposion: CFD – die Zukunft der Sicherheitstechnik

22.-25. Mai 2011

- **JP-4- und DTBP-Poolfeuer als Testfeuer; multiple Tankfeuer (Buncefield)**
- **Physikalische Vorgänge in Pool-, Lachen- und Tankfeuern**
- **Bisherige und neue Modelle**
- **Experimentelle Untersuchungen**
- **CFD-Simulation**
  - **Flammentemperaturen**
  - **Surface *E*missive *P*ower (SEP)**
  - **Bestrahlungsstärke und kritische thermische Abstände**
- **Folgerungen und Ausblick**

Einführung

JP-4-Poolfeuer (d = 25 m)
(Testfeuer)

DTBP-Poolfeuer (d = 3.4 m)
(Testfeuer)

Buncefield, nahe London, 11.12.2005

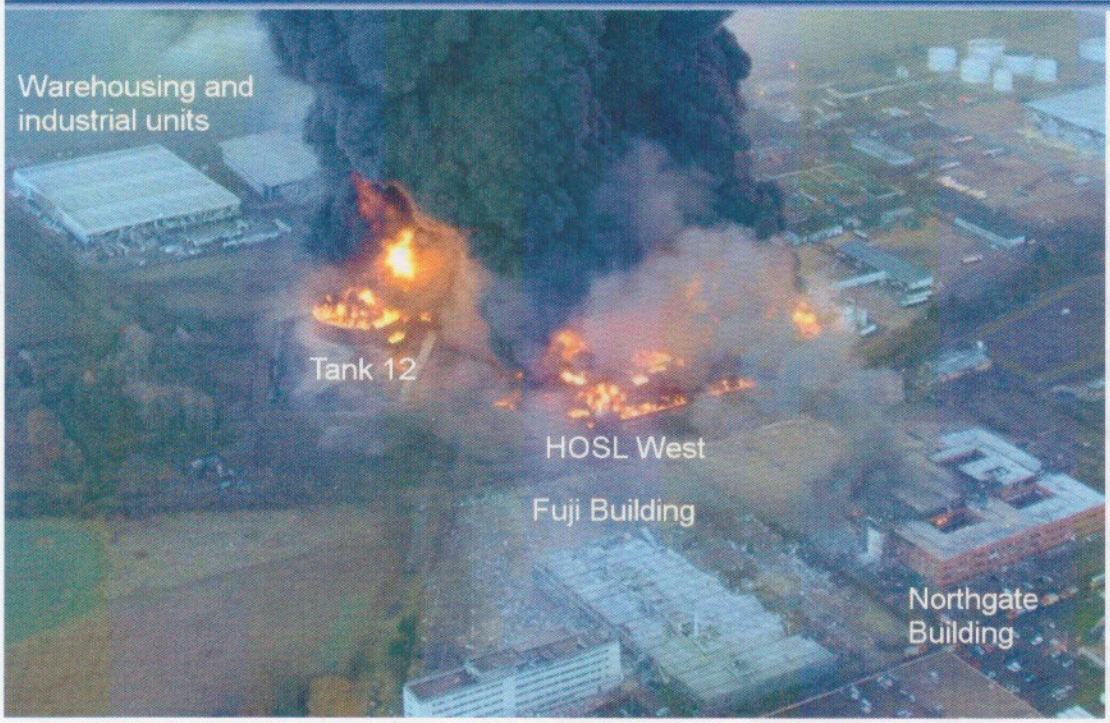

Buncefield Anlage am ersten Tag des Feuers. Es ist zu erkennen, dass auch das ≈150 m entfernte Northgate Gebäude (rechts unten im Bild) an der Ecke der Seite brennt, die den multiplen Tankfeuern gegenüber liegt.

Physikalischer Vorgänge

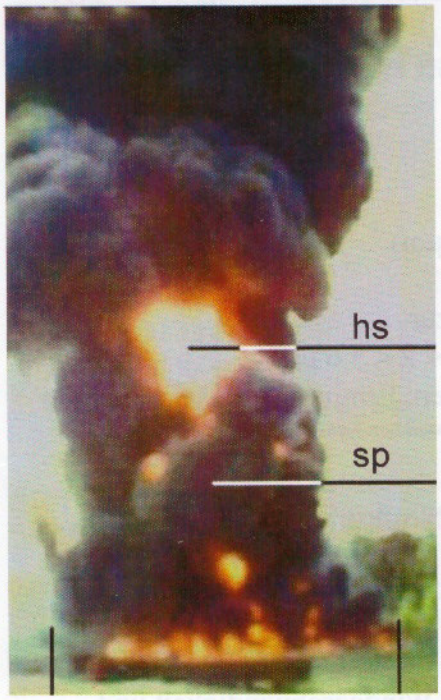

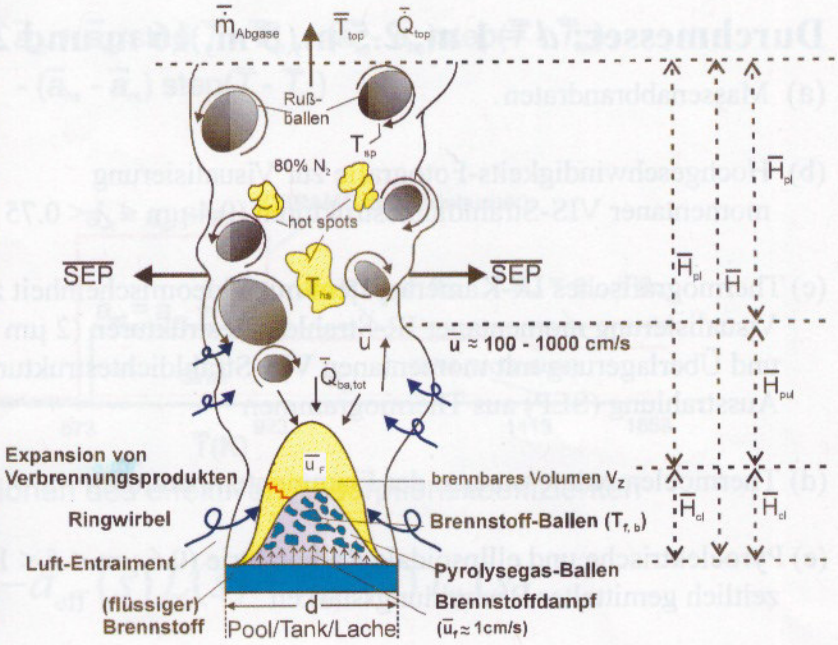

Physikalische Vorgänge in Pool-, Lachen- und Tankfeuern

Bisherige und neue (N) Konsequenzmodelle (Thermische Strahlung)

Punktquellen-Strahlungs Modell (PSM) — *API 521* (1969)

Oberflächen-Strahlungsmodelle

Zylinderflammen-Strahlungsmodell (SFM) — *Seeger* (1971)

Modifiziertes Zylinderflammen Strahlungsmodell (MSFM) *Yellow Book* (1992)

Luminous Spots - Soot Zonen-Modell — *Mudan* (84,95,2002)

(N) OSRAMO II, OSRAMO III (*O*rganized *S*tructures *RA*diation *Mo*dels) — *Schönbucher et al.* (85, 91, 2006)

(N) Strahlungsmodell (*SEP*(*x*)) — *Raj* (2007)

(N) Strahlungsmodell (*SEP*(*x*)) — *Fay* (2006)

(N) Transiente Modelle: CFD-Simulation — *Schönbucher et al.* (seit 2000)

z.B. *SEP*(*x*,*y*,*t*), *T*(*x*,*y*,*z*,*t*)

Experimentelle Untersuchungen

Brennstoffe: n-Pentan, Superbenzin, Normalbenzin, Diesel, JP-4, LNG, DTBP

Durchmesser: d = 1 m, 2.5 m, 8 m, 16 m und 25 m

(a) Massenabbrandraten

(b) Hochgeschwindigkeits-Fotografie zur Visualisierung momentaner VIS-Strahldichtestrukturen ($0.4\ \mu m < \lambda < 0.75\ \mu m$)

(c) Thermografisches IR-Kamerasystem mit Videomischeinheit zur Visualisierung momentaner IR-Strahldichtestrukturen ($2\ \mu m < \lambda < 5.6\ \mu m$) und Überlagerung mit momentanen VIS-Strahldichtestrukturen; Ermittlung der spezifischen Ausstrahlung (SEP) aus Thermogrammen

(d) Thermoelementmessungen der Flammentemperaturen

(e) Pyroelektrische und ellipsoidale Radiometrie ($0.6\ \mu m < \lambda < 15\ \mu m$) zur direkten Messung zeitlich gemittelter Bestrahlungsstärken

(f) Meteorologische Messstation zur Erfassung insbesondere von Windgeschwindigkeit und Windrichtung

Neue Konsequenzmodelle (CFD Simulation)

Erhaltungs-Gleichungen

Impuls
Energie
Gesamtmasse
Speziesmassen

Solver

Coupled - CFX
Segregated/
Coupled - FLUENT

Verbrennungsmodelle

Mehrschritt-Chemie über
Assumed PDF-Ansätze mit laminaren flamelets
(112 Spezies, 800 Reaktionen) für JP-4
(20 Spezies, 42 Reaktionen) für Methan

Turbulenzmodelle

- LES Large-Eddy-Simulation - ANSYS FLUENT mit dynamischem Smagorinsky-Lilly-Subgridmodell
- Scale Adaptive Simulation (SAS) - ANSYS CFX

Strahlungsmodelle

- Monte Carlo Methode - CFX
- Discrete Ordinates Methode - FLUENT
  - Modellierung des Absorptionskoeffizienten

Rußmodelle

- Magnussen - CFX
- Lindstedt - CFX
- Tesner - FLUENT
- Moos-Brookes - FLUENT

Neue Konsequenzmodelle (CFD Simulation)

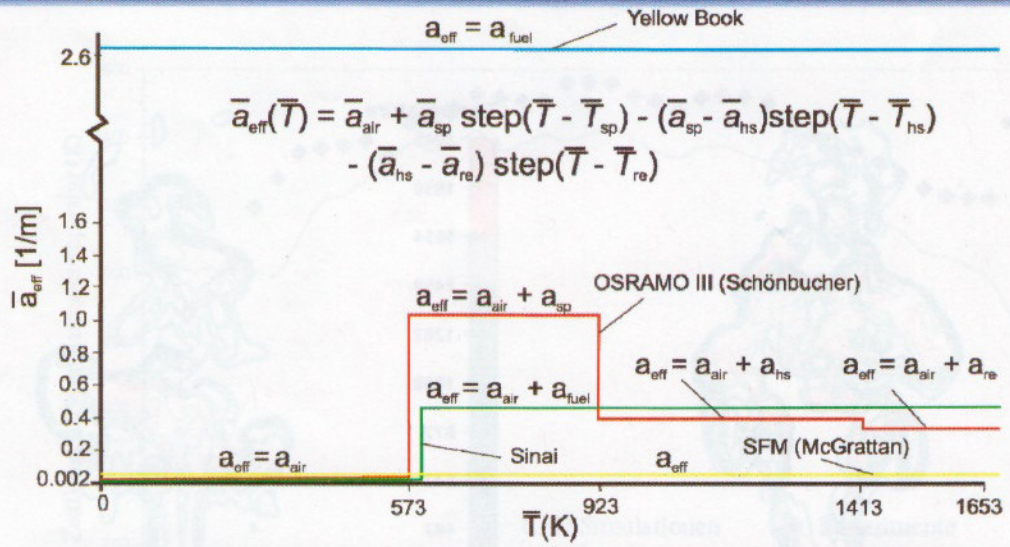

Mehrstufenfunktionen des effektiven Absorptionskoeffizienten

$$\frac{dL}{ds} = -a_{\text{eff}}(s)\,L(s) + a_{\text{eff}}(s)\,L_b(s)$$

Strahlungstransportgleichung

Neue Konsequenzmodelle (CFD Simulation)

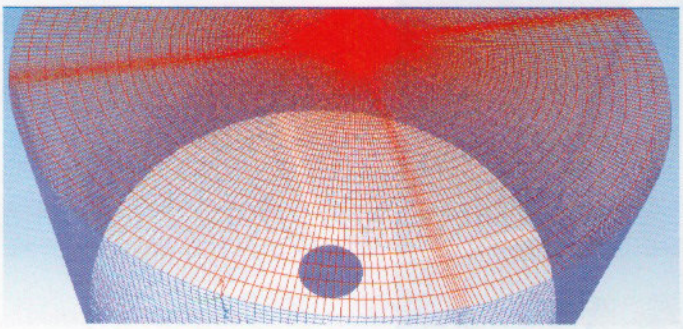

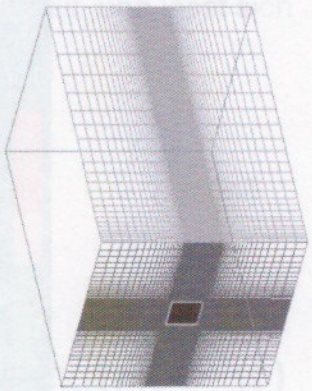

(a) (b)

Block-strukturiertes Gitter zur Simulation von (a) JP-4 Poolfeuern (d = 25 m) und (b) DTBP-Poolfeuern (d = 3.4 m)

Zeitschritt: 10^{-4} s < Δt < 10^{-6} s für ausreichende iterative Konvergenz und Stabilität

Anzahl der Zellen: $N_{max} \approx 15\,000\,000$

Flammentemperaturen

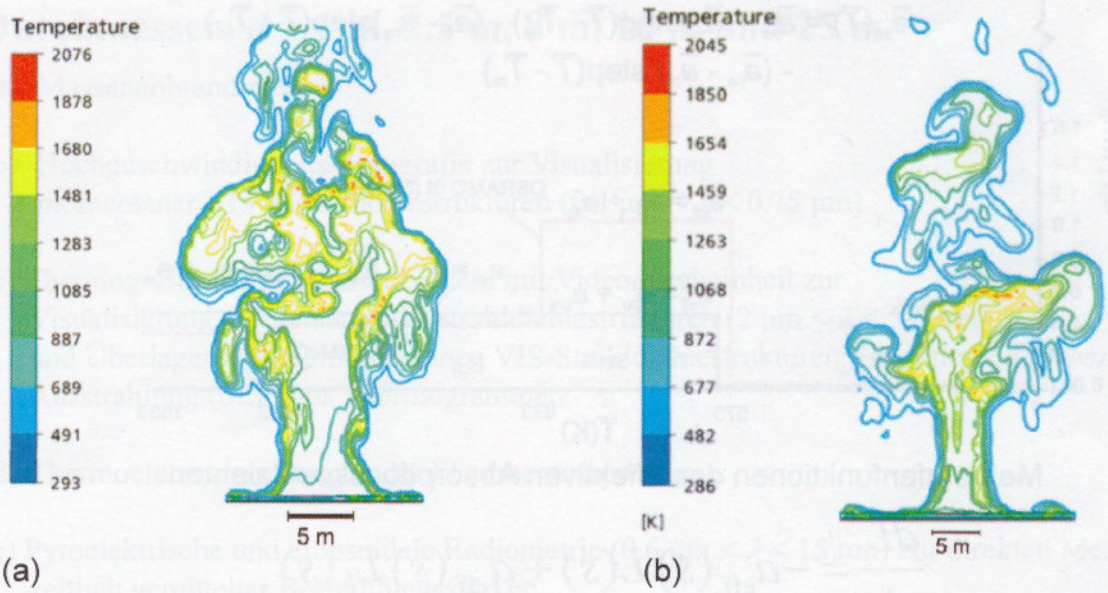

CFD vorhergesagte momentane Temperaturfelder von JP-4 Poolfeuern
(a) d = 16 m; (b) d = 25 m

Flammentemperaturen

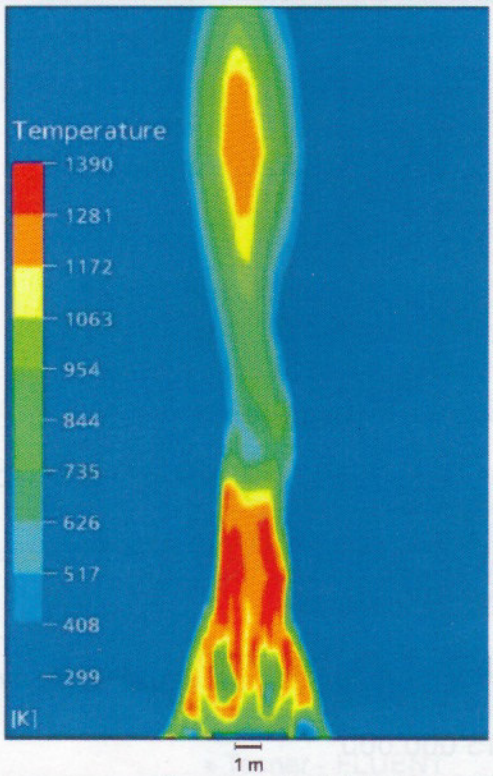

CFD-vorhergesagtes momentanes Temperaturfeld eines DTBP-Poolfeuers (d = 3.4 m)

Flammentemperaturen

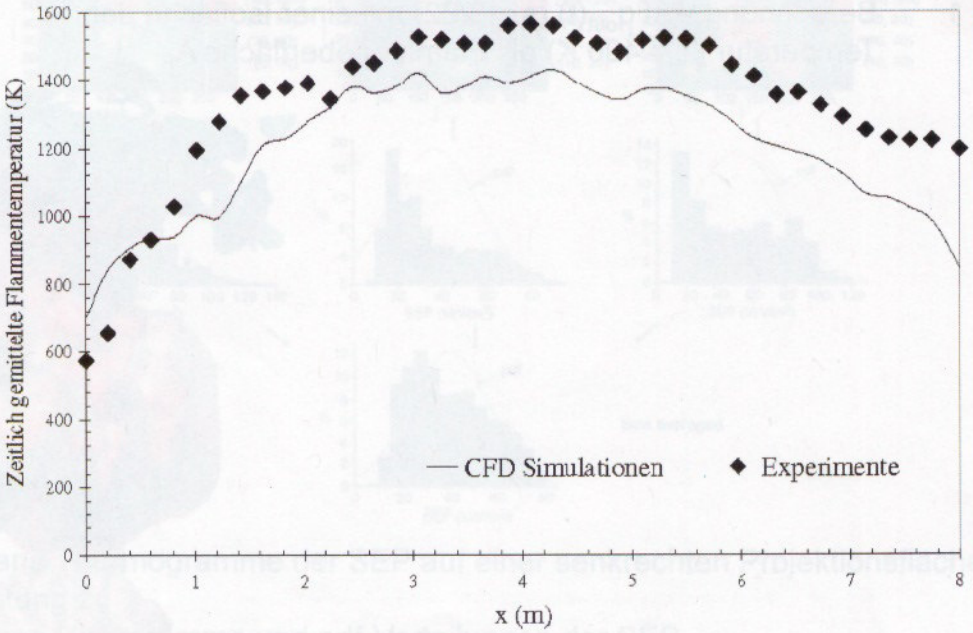

Zeitlich gemittelte axiale Flammentemperaturprofile eines DTBP-Poolfeuers (d = 3.4 m)

Spezifische Ausstrahlung (SEP)

SEP ist eine *abgeleitete* Größe, abhängig von A_F, Flammenkontur, und lässt sich berechnen nach:

$$\overline{SEP}_{CFD} \equiv \langle \overline{q_{out}} \rangle = \frac{\sum_{1}^{N_T} \langle q_{out}(t) \rangle}{N_T} \quad , \quad \text{mit}$$

$$q_{out}(t) = (1-\varepsilon_{tot}(t)) \int_{\vec{s}\cdot\vec{n}<0} L(t)\,\vec{s}\,\vec{n}\,d\Omega \; + \varepsilon_{tot}(t)\sigma T^4(t) \quad ,$$

wobei $\vec{n} \perp A_F$

q_{out} : austretender Wärmefluss an derFlammenoberfläche [kW/m²]

ε_{tot} : gesamter Emissionsgrad

< > : örtl. gemittelt, über A_F

Spezifische Ausstrahlung (SEP)

Weg 1: Berechnung von $q_{out}(t)$ (s. 13/22) mit einer Isofläche der Temperatur (T = 400 K) als Flammenoberfläche A_F

CFD vorhergesagte, momentane SEP(x,y,t) auf einer Isofläche der Temperatur von T = 400 K für ein JP-4 Poolfeuer (d = 16 m)

Spezifische Ausstrahlung (SEP)

Weg 2: Berechnung von $q_{out}(t)$ (s. 13/22) mit einer senkrechten Projektionsfläche $A_{x,y}$ als Flammenoberfläche A_F

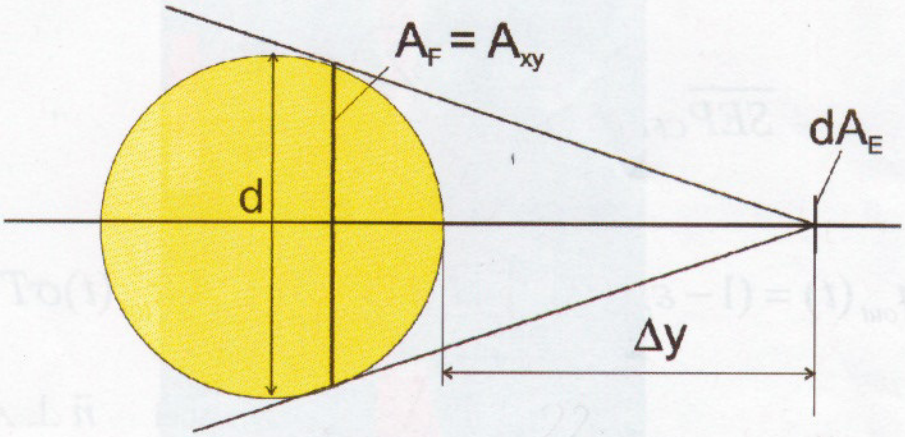

$$\overline{SEP}(d) \equiv <\overline{SEP}_{i,j}(d)> = \frac{\sum_i \sum_j \overline{SEP}_{i,j}\, a_x}{\sum_i \sum_j a_x} \quad \text{, mit} \quad \overline{SEP}_{i,j} \equiv \frac{\sum_1^{N_T} SEP_{i,j}(t)}{N_T} \; .$$

a_x : Pixelfläche in einem Thermogramm

Spezifische Ausstrahlung (SEP)

Weg 2:

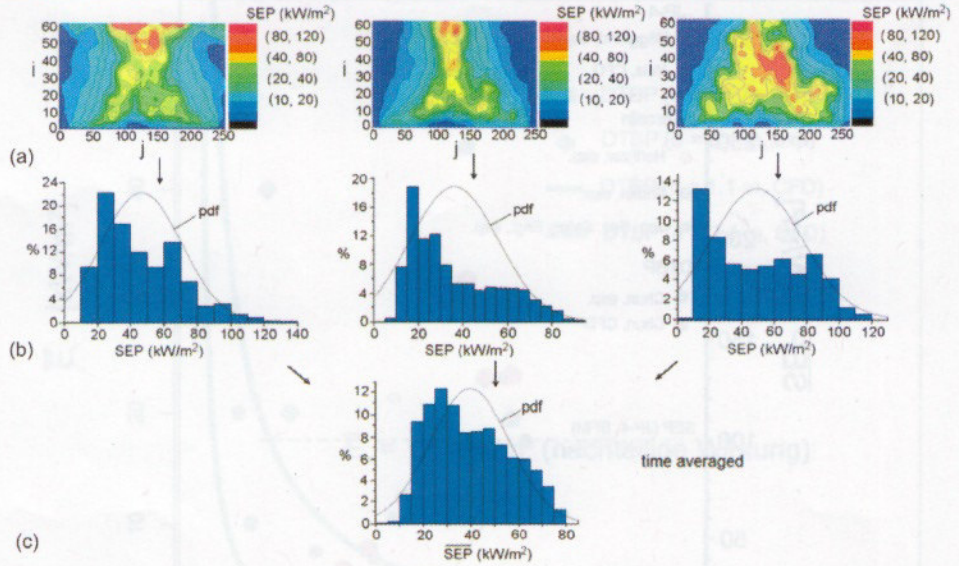

(a)Momentane Thermogramme der SEP auf einer senkrechten Projektionsfläche A_{xy} zu Strahlrichtung z
(b)Momentane Histogramme und pdf-Verteilungen der SEP
(c)Zeitlich gemitteltes Histogramm und zeitlich gemittelte pdf-Verteilung der SEP, jeweils vorhergesagt mit CFD für ein JP-4 Poolfeuer (d = 16 m)

Spezifische Ausstrahlung (SEP)

Weg 3:

$$\overline{SEP}_{CFD} = \frac{\overline{E}_{CFD}(\Delta y / d)_{\Delta y/d \to 0}}{\tau_{at}\,\alpha_E\,\varphi_{E,F}(\Delta y / d)_{\Delta y/d \to 0}}$$

Bestimmung der Bestrahlungsstärke $\overline{E}_{CFD}$ mit *virtuellen* Radiometern in Abhängigkeit von Δy/d.

Atmosphärischer Transmissiongrad: $\tau_{at} \le 1$

Absorptionsgrad des Empfängerflächenelementes: $\alpha_E \le 1$

CFD-Simulation – Validierung

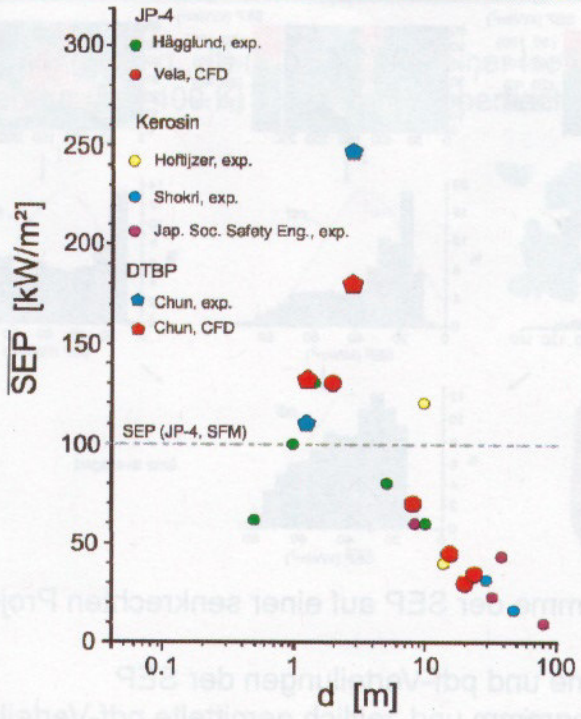

Gemessene und CFD-vorhergesagte SEP von Kohlenwasserstoff- und DTBP-Poolfeuern in Abhängigkeit des Pooldurchmessers

Bestrahlungsstärke E und krititsche thermische Abstände Δy_{crit}

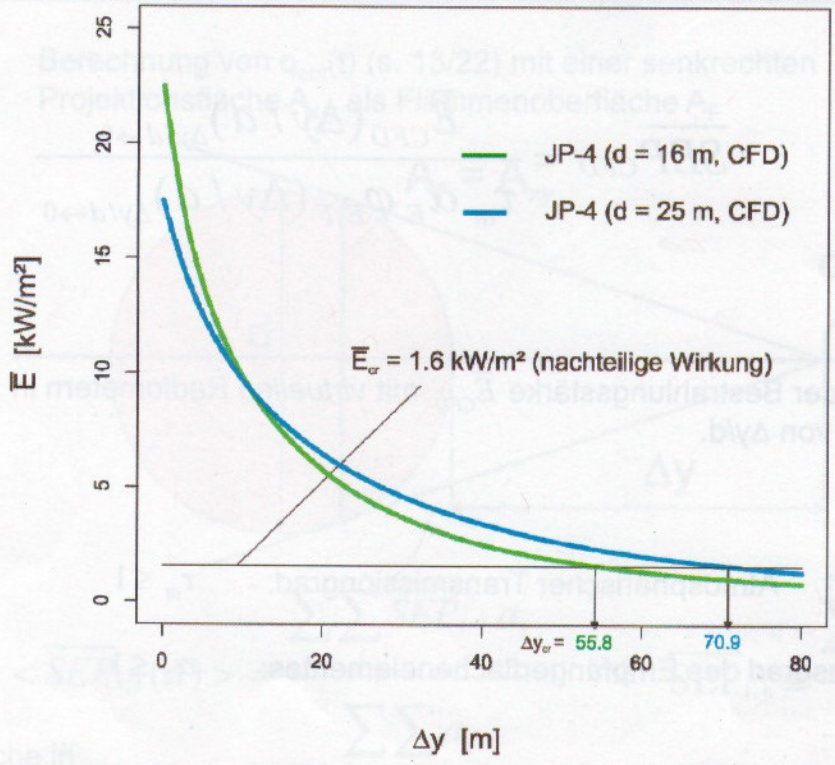

Kritische thermische Abstände Δy_{cr} von JP4-Poolfeuern

Bestrahlungsstärke E und krititsche thermische Abstände Δy_{crit}

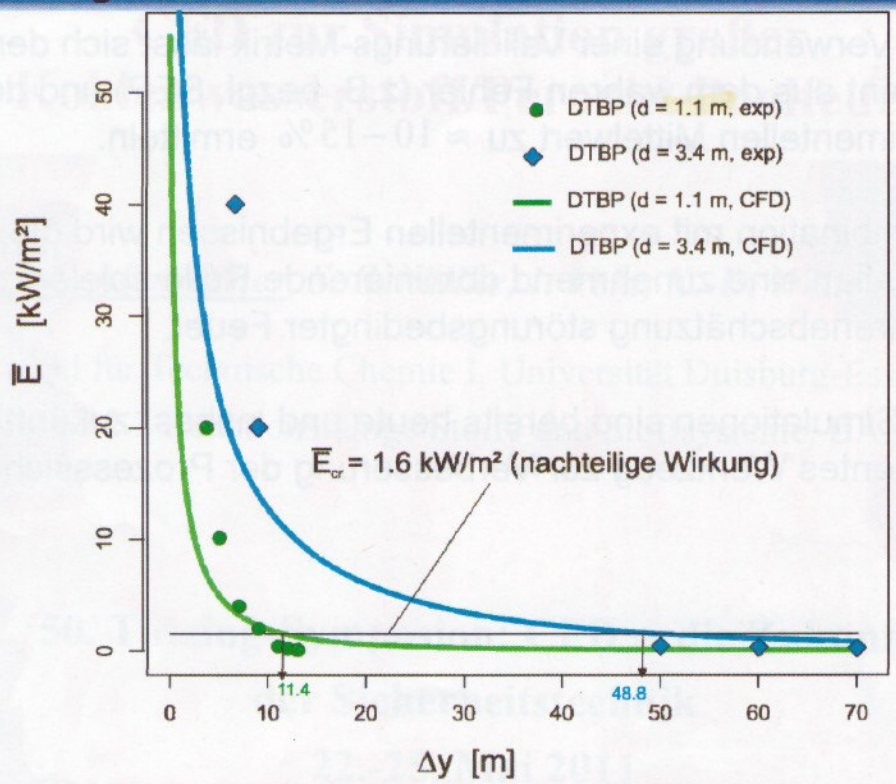

Kritische thermische Abstände Δy_{cr} von DTBP-Poolfeuern

Folgerungen und Ausblick

(I) *Bisher* angewandte Modelle (insbes. SFM, MSFM) sind teilweise ungeeignet.

(II) *CFD-Simulationen* sind gut geeignet zur Berechnung charakteristischer Eigenschaften (*SEP*, *E*, Δy_{cr}) auch größerer KW- und Peroxid-Feuer.

(III) Modellierung eines effektiven Absorptionskoeffizienten sowie einer nicht-Gleichgewichtschemie, wie insbes. Flamelet-Modelle ist für eine erfolgreiche CFD-Simulation von großer Bedeutung

(IV) *Bisherige* Worst Case Annahmen sind zu überdenken

(V) Datenmangel (insbes. *H*, *SEP*, *E*) bei größeren Einzel- und multiplen Lachen-, Pool- und Tankfeuern sollten beseitigt werden.

Folgerungen und Ausblick

(VI) Unter Verwendung einer Validierungs-Metrik lässt sich der Quotient aus dem wahren Fehler (z.B. bezgl. SEP) und dem experimentellen Mittelwert zu $\approx 10-15\%$ ermitteln.

(VII) In Kombination mit experimentellen Ergebnissen wird die CFD-Simulation eine zunehmend dominierende Rolle spielen zur Gefahrenabschätzung störungsbedingter Feuer.

CFD-Simulationen sind bereits heute und insbes. zukünftig ein exzellentes Werkzeug zur Verbesserung der Prozesssicherheit.